LARGE ANTENNA MEASUREMENT AND COMPENSATION TECHNIQUES *

Y. RAHMAT-SAMII
Jet Propulsion Laboratory
California Institute of Technology
Pasadena, CA

*Published in the Proceedings of the 11th ESTEC Antenna Workshop on Antenna Measurements held in Gothenburg, Sweden, June 20-22, 1988.

ABSTRACT

Antennas in the range of 20 meters or larger will be an integral part of future satellite communication and scientific payloads. In order to commercially use these large, low sidelobe and multiple-beam antennas, a high level of confidence must be established as to their performance in the 0-g and space environment. It is also desirable to compensate for slowly varying surface distortions which could result from thermal effects. An overview of recent advances in performing rf measurements on large antennas is presented with emphasis given to the application of a space-based far-field range utilizing the Space Shuttle. The concept of surface distortion compensation is discussed by providing numerical and measurement results.

1. INTRODUCTION

It is very likely that antennas in the range of 20 meters or larger will be an integral part of future satellite communication and scientific spacecraft payloads. For example, Fig. 1 depicts the conceptual evolution of the Land Mobile Satellite System which is anticipated to evolve from utilizing approximately 6-9 meter reflectors to 55 meter reflectors in the era spanning the late 1980's to early 2000's. In order to commercially use these large, low sidelobe and multiple-beam antennas, a high level of confidence must be established as to their performance in the 0-g and space environment. Certain ground (1-g) testing can be performed to validate the workability of different segments of such large structures; however, it will be a formidable task to characterize the performance of the entire structure on the ground.

For this reason, an overview of rf measurement techniques applicable to large antennas is provided. Attention will be focused on a conceptual study which has recently been initiated with the intent to describe an experiment aboard the Space Shuttle which would demonstrate the deployment reliability of the antenna structure, measure thermal and dynamic structural characteristics, and verify performance specification under all expected conditions.

The concept of surface distortion compensation is discussed by reviewing the applicability of different approaches. A technique based on the application of a compensating array feed is presented. Numerical results and measured data will be shown to demonstrate the utility of this compensation technique.

2. AN OVERVIEW OF MEASUREMENT TECHNIQUES

In the last twenty years significant developments have been reported on the subject of antenna measurements. Most importantly due to the improvement of

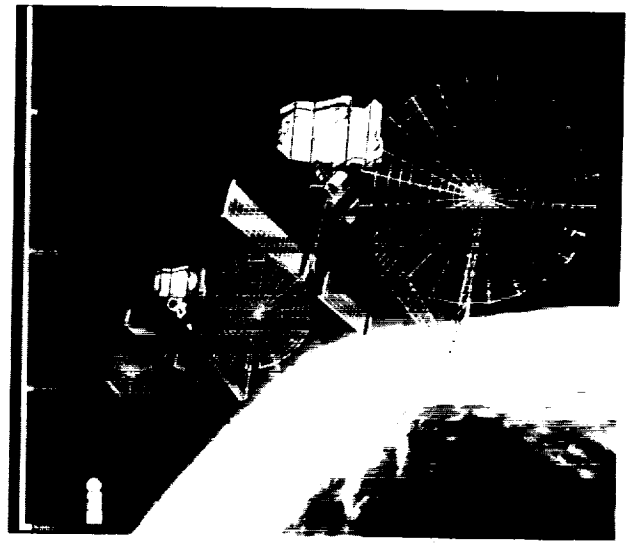

FIG. 1. Evolution of the proposed Land Mobile Satellite System (LMSS).

measurement systems in accurately measuring amplitude and phase, new methodologies have been advanced which have completely changed the nature of the classical far-field measurements. Among these new measurements concepts which are also applicable to large antenna measurements, one can refer to the following concepts [1-7]:

* Near-Field measurements
* Compact range measurements
* Modern far-field measurements
* Fly by measurements
* Microwave holographic measurements
* Integrated photogrammetric and rf measurements
* Integrated computer analysis and rf measurements
* In-space rf measurements
* Combination of the above techniques

Fig. 2 provides a block diagram for interrelating these measurement techniques. There is a considerable amount of published material on each of the above techniques to demonstrate their merits, advantages and disadvantages. It is the users responsibility to acquire an in-depth appreciation of the applicability of each of the above measurement concepts for the problem at hand. This means that the user should carefully identify what characteristics of the antenna need be measured for a given application and above all to identify the required accuracy in measuring the antenna parameters of interest. In the following, examples are given for selected measurement techniques applicable to large antennas based on the author's experience.

3. NEAR-FIELD MEASUREMENTS

Near-field measurement techniques have enjoyed much development and utilization among many rf measurement engineers. There are many organizations worldwide that use near-field measurement techniques on routine bases [1]. Here, two examples are given on the application of near-field measurement techniques to large deployable antennas.

The 4.8-meter mesh deployable antenna of the Galileo spacecraft has been measured in the near-field plane-polar facility at JPL. This facility has the unique characteristic which allows the skyward mounting of the antenna on the positioner. It is essential that large mesh deployable antennas be measured in this position if any meaningful rf measurements are to be performed on the ground. The reader is referred to [8] for a detailed description of this measurement. As shown in Fig. 3, the antenna rotates on its axis as the probe is advanced in the radial direction.

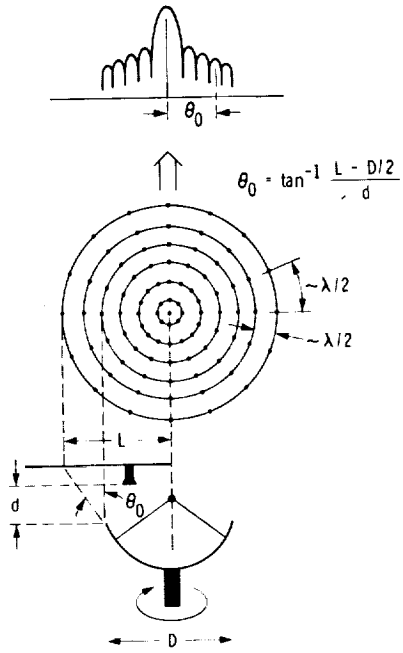

FIG. 3 Plane-polar measurement technique.

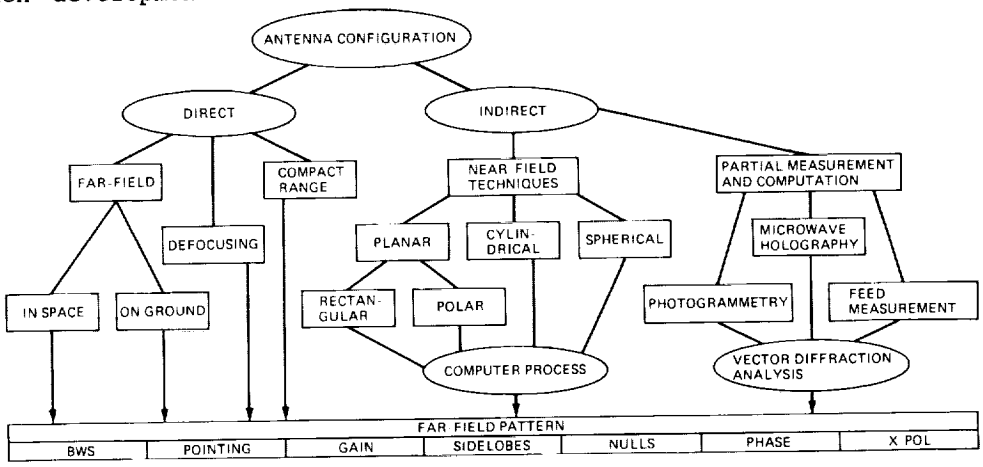

FIG. 2. A block diagram for inter-relating various measurement techniques.

The near-field data are collected on concentric circles which are then transformed to the far field using either Jacobi-Bessel expansion or an FFT algorithm. A photo of the deployed antenna in the near-field chamber is shown in Fig. 4 and a representative far-field pattern is depicted in Fig. 5.

The largest deployable antenna commercially measured was the 15-meter hoop-column mesh antenna built by Harris corporation under a contract to NASA/LaRC [9]. This antenna was measured at the near-field facility of Martin-Marietta in a joint effort supported by LaRC/JPL/Martin-Marietta. The purpose of the measurement has been to demonstrate the utility of large mesh deployable antennas, to test the newly developed overlapping microstrip array feed cluster, and to test the accuracy of the computational techniques. A photo of this antenna deployed in the near-field chamber is shown in Fig. 6.

FIG. 4. Mesh deployable 4.8 meter Galileo antenna in the near-field facility.

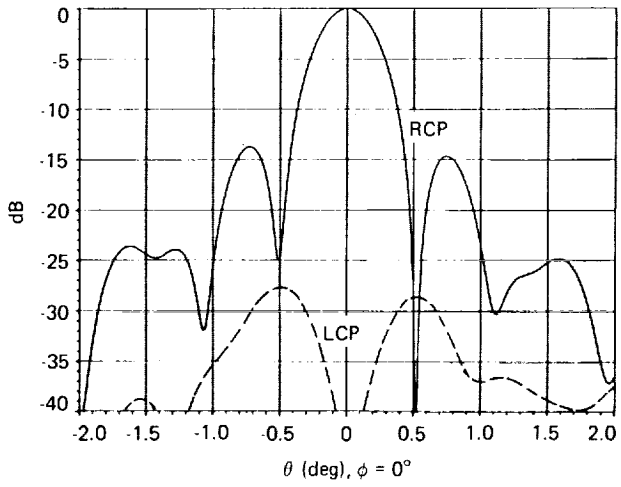

FIG. 5. Constructed far-field patterns for the circularly polarized Galileo antenna at 8.415 GHz.

It is important to realize that this hoop-column reflector antenna consists of four sub-apertures each of which is an offset parabolic surface. Again as seen from Fig. 6, the antenna is positioned skyward in the chamber which utilizes a rectangular near-field measurement setup. In order to correlate the results of the measurement with those based on computational techniques, a set of photogrammetry measurements was conducted to identify the location of the target points mounted on the reflector surface (Fig. 7). Fig. 8 shows the results of the comparison between the measurements and computations using the ideal parabolic surface. Also shown in Fig. 9 are the measured far-field patterns constructed from the near-field measurements using the overlapping feed cluster.

For large antennas, it appears that the near-field planar technique has the advantage over cylindrical and spherical techniques because of its simpler mechanical setup for the skyward positioning of the antenna. Recently attempts have been made to consider the utility of the combined plane-polar and

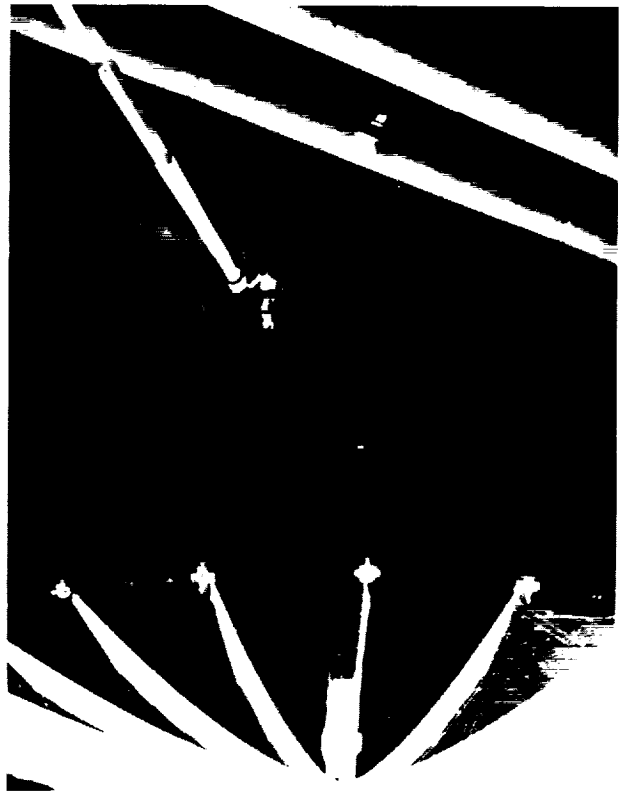

FIG. 6. 15-meter hoop-column antenna in Martin Marietta near-field facility.

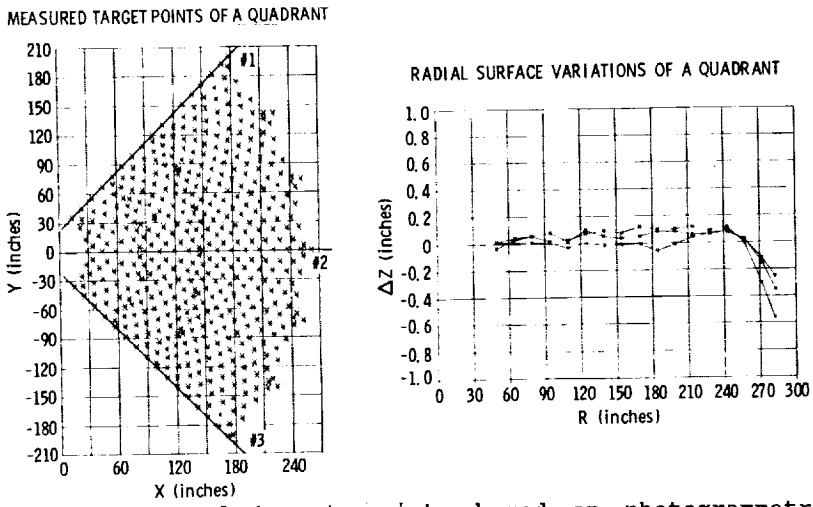

FIG. 7. Measured target points based on photogrammetry technique. ΔZ is the surface deviation from the best fit paraboloid.

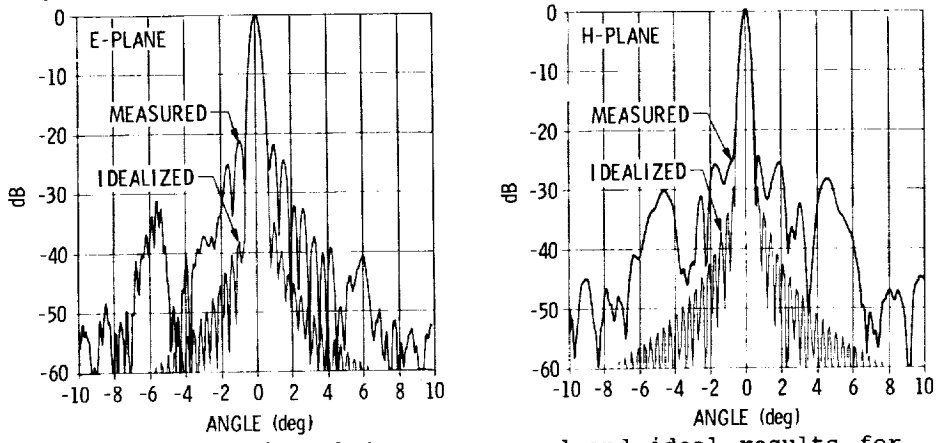

FIG. 8. Comparison between measured and ideal results for the 15-m antenna at 7.73 GHz.

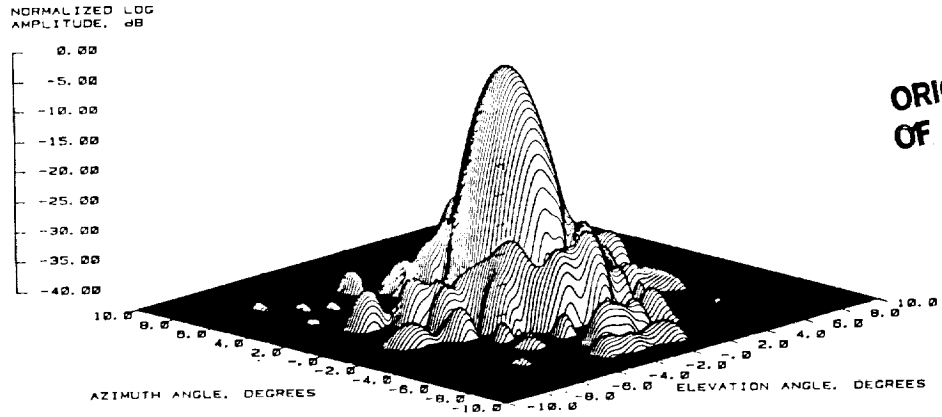

FIG. 9. Measured far-field pattern for the 15-m antenna using the overlapping feed cluster at 2.23 GHz.

cylindrical near-field technique as depicted in Fig. 10 [10]. Once operational this combined technique has the advantage of reducing the needed area of the near-field measurement of the plane-polar and the added feature of allowing the construction of the far-field pattern in wider angular range than is typically obtainable from the planar near field alone. The usefulness of this combined technique can be further improved by utilizing the modulated scattering approach for the reduction of the measurement time [11]. It is anticipated that such a measurement apparatus could be mounted aboard the Space Station for future in-space testing and verification of large antenna systems.

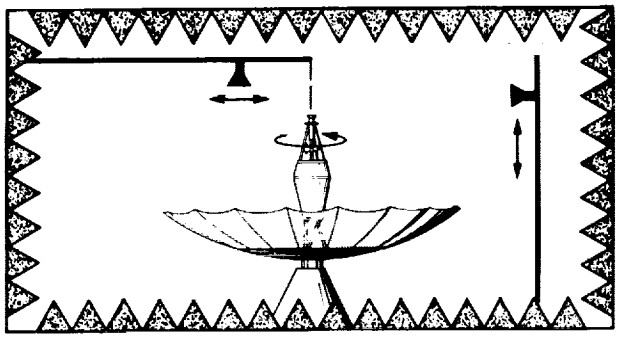

FIG. 10. A combined plane-polar and cylindrical near-field measurement technique.

4. MICROWAVE HOLOGRAPHIC METROLOGY

As mentioned before, photogrammetry has been used to determine the surface profile of large antennas. This technique utilizes optical cameras to take several photographs of the antenna covered by many target points. These photographs are then processed to finally identify the shape of the reflector surface [4].

Recently, attention is given to microwave holographic techniques which allow the determination of the reflector surface shape based on microwave measurements. This technique is unique in that it can be used in conjunction with far-field, near-field and compact range measurement techniques. Fig. 11 shows the steps involved in applying microwave holographic metrology for antenna diagnosis. The essence of the technique is based on the observation that the antenna far-field is proportional the Fourier transform of a function which is related to the induced current on the reflector surface. Therefore, once the amplitude and phase of the far-field pattern are measured in an appropriate angular interval, they can be used to determine the surface profile. This technique has been applied very successfully for measuring many large ground antennas worldwide [12,13,14]. It is expected that with some refinements the technique should also be applicable to the space antennas.

As an example, Fig. 12 shows the results of a recent measurement performed on one of the 64 meter antenna of NASA/JPL/Deep Space Network (DSN) reflector antennas. A photo of this antenna is shown in Fig. 13. It is anticipated that application of the microwave holographic metrology will

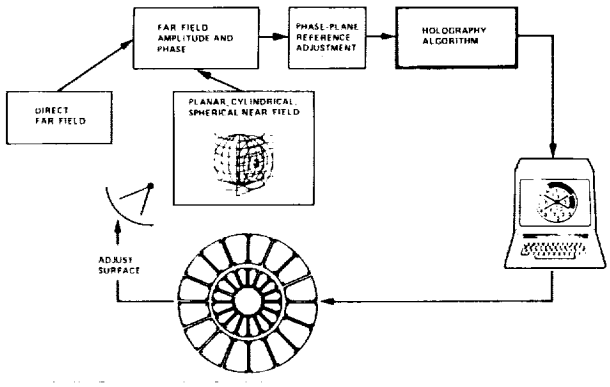

FIG. 11. Steps in applying microwave holographic diagnosis.

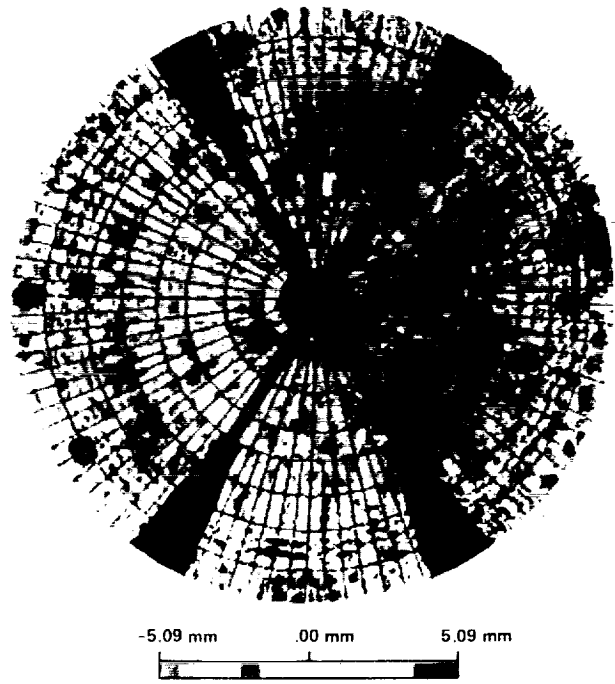

FIG. 12. Surface error map for the DSN reflector antenna.

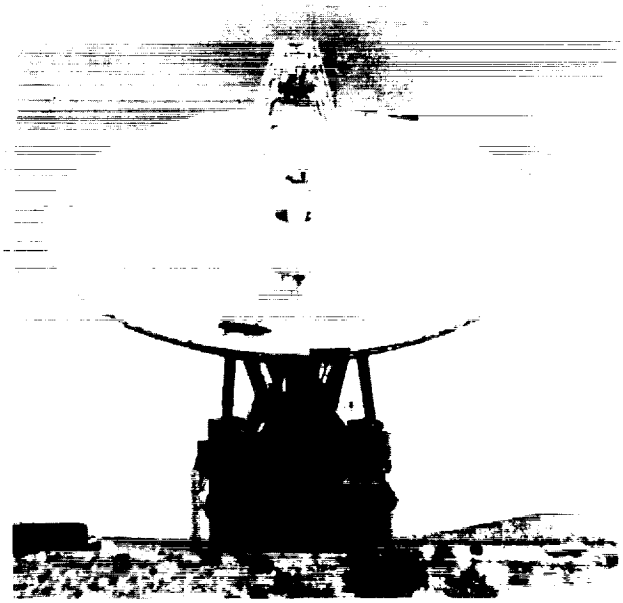

FIG. 13. NASA/JPL 64-m Deep Space Network (DSN) antenna.

attract attention in diagnosis of large deployable antennas either measured in near-field facilities or far fields. As will be discussed later, the outcome of surface diagnostics can be used in applying surface distortion compensation.

As mentioned earlier, microwave holographic reconstruction may be used in conjunction with near-field measurements providing a useful diagnostic tool. This hybrid approach of combining near-field measurement and holographic reconstruction would allow an in-depth evaluation of the accuracy of the holographic technique because the spherical near-field measurement, in particular, provides accurate amplitude and phase far-field patterns for the entire angular range. The steps of this hybrid approach are depicted in Fig. 14.

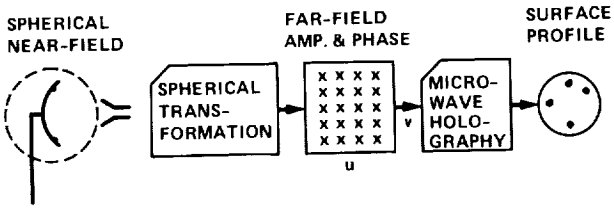

FIG. 14. Steps in performing Microwave Holographic Diagnosis using spherical near-field measurements.

Under controlled conditions, two sets of spherical near-field measurements were performed on a 156-cm reflector at 11.3 GHz. In the first measurement, the antenna was measured in its existing condition while in the second measurement, four bumps of different sizes and heights were attached at several locations to the reflector surface (see Fig. 15). These measured near-field data were used to generate the far-field amplitude and phase patterns of the reflectors using a spherical near-field to far-field algorithm. Then the steps of the block diagram shown in Fig. 14 were employed to generate the surface profiles.

Similar steps were followed for both the original and bumped reflectors. However, in order to demonstrate how successfully the bumps were recovered, the results of original and bumped reflectors were used to obtain the final result and to remove the contamination due to the reflector's original imperfection. To this end, the generated holographic surface profiles of the two measurements were subtracted to essentially remove the effects due to the original surface imperfection, struts diffraction, feed misalignments, nonspherical phase pattern of the feed, and other factors. Results are shown in Fig. 16 using the contour plot presentation, which clearly demonstrates how well the four attached bumps are recovered.

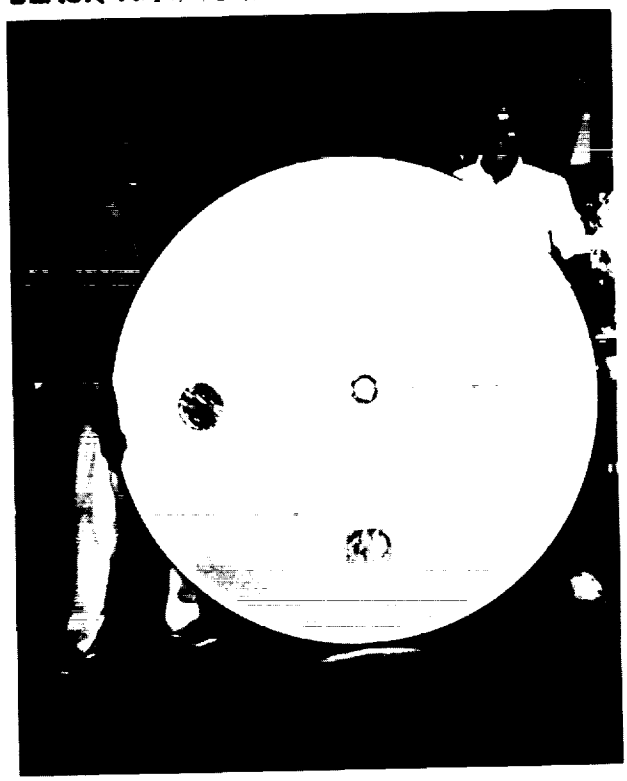

FIG. 15. Antenna with four attached bumps of different sizes and locations.

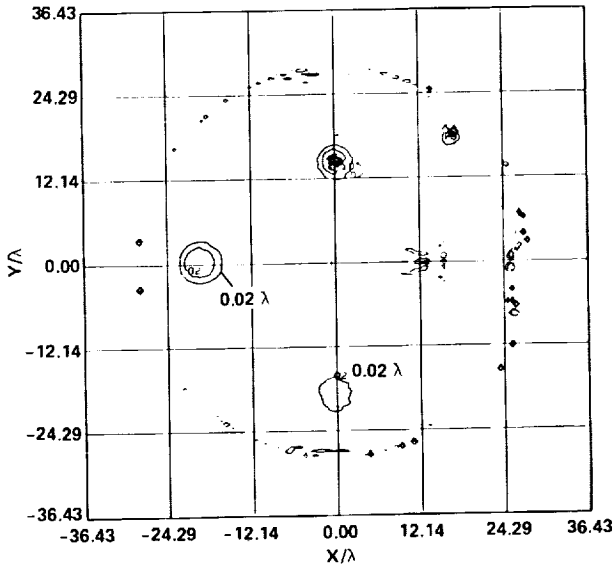

FIG. 16. Reconstructed surface profile after subtraction (11.3 GHz).

5. SHUTTLE BASED RF MEASUREMENTS

Since the actual space environment can only be achieved in space, special consideration is being given to the rf far-field pattern measurements of large antennas aboard the Space Shuttle. This measurement should provide the ultimate characterization for the antenna performance (Fig. 17).

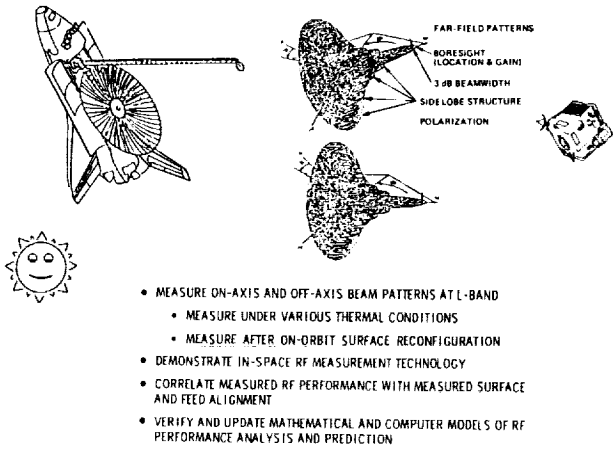

- MEASURE ON-AXIS AND OFF-AXIS BEAM PATTERNS AT L-BAND
- MEASURE UNDER VARIOUS THERMAL CONDITIONS
- MEASURE AFTER ON-ORBIT SURFACE RECONFIGURATION
- DEMONSTRATE IN-SPACE RF MEASUREMENT TECHNOLOGY
- CORRELATE MEASURED RF PERFORMANCE WITH MEASURED SURFACE AND FEED ALIGNMENT
- VERIFY AND UPDATE MATHEMATICAL AND COMPUTER MODELS OF RF PERFORMANCE ANALYSIS AND PREDICTION

FIG. 17. Spaced-based RF experiment objectives aboard the Space Shuttle.

Several potential scenarios have been considered and the relative merit of each of them are shown in qualitative manner in Fig. 18. Among all these possibilities the application of the scenario shown in the last row appeared most feasible. The rf experiment is anticipated to be performed on a 20-meter offset reflector at L-band using the Remote Mini-Flyer, a NASA-developed reusable and retrievable spacecraft (a modified Spartan), as the carrier for an rf beacon. This beacon is used to illuminate the antenna in a similar fashion as one does in the ground-based far-field ranges using transmit illuminators. An artist's rendition of this spaced-based experiment is depicted in Fig. 19.

Among the several rf measurement concepts studied, application of a far-field arrangement with an RF illuminator mounted aboard the free-flyer appeared to be the most feasible. Furthermore, in order to reduce the cost of the experiment, it has been anticipated that no gimbal mechanism will be used to accurately control the position of the antenna with respect to the illuminator. Instead, the relative

TECHNIQUES	CONFIGURATION	COMPLEXITY	USEFULNESS	COST
NEAR FIELD TECHNIQUES		☹	😐	☹
COMPACT RANGES		😕	😐	☹
BEACON ON THE GROUND		😐	☹	☹
RECEIVING CITIES ON THE GROUND		😐	☹	😐
RADIO STAR SOURCES		😐	😐	😐
GEO SATELLITE SOURCES		😐	😐	😐
FREE-FLYER AS A BEACON		😐	😐	😐

FIG. 18. A qualitative comparison of different measurement techniques aboard the Space Shuttle.

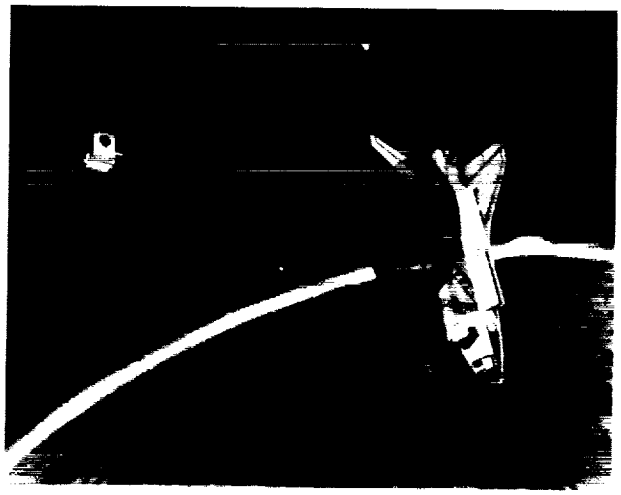

FIG. 19. An artist's rendition of the proposed large antenna Shuttle experiment.

motion of the Shuttle and free-flier in a controlled manner will be utilized to provide the angular range of interest. Depending on what the exact covered u-v space will be, several scenarios could be considered.

Since without any gimbal system it will be impractical to measure antenna patterns in specified ϕ cuts, one may have to perform the measurement in a specified u-v angular range in a time period in which the antenna structure is not changed appreciably from an rf viewpoint. Fig. 20 shows the possibility of measuring very dense but nonuniformly measured data points from which the needed ϕ-cuts or contour patterns can be constructed. If it is proved that the possibility of measuring a very dense set of data may not be realistic, an alternate scheme should be available. This alternate scheme is depicted in Fig. 21, which assumes that

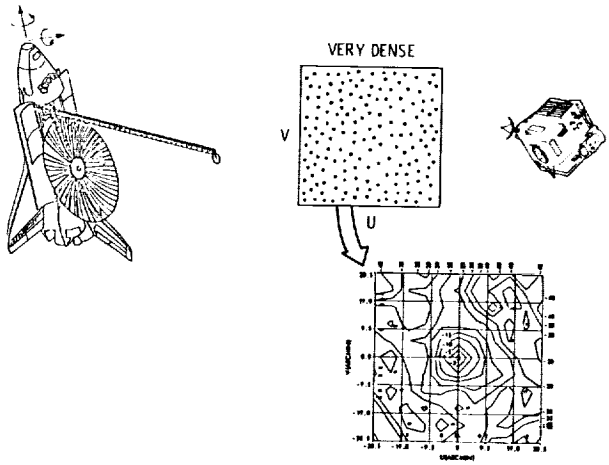

FIG. 20. Schematic of nonuniform and very densely measured sampled points.

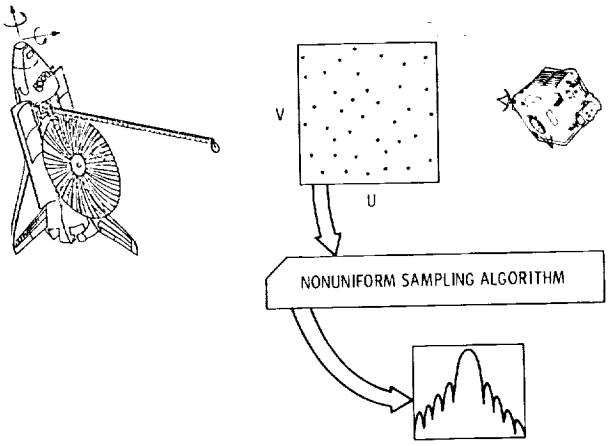

FIG. 21. Schematic of a nonuniform and relatively sparsely measured sampled points.

the measured (amplitude and phase) are obtained at relatively sparse and nonuniformly distributed u-v points. The question is, then, whether or not one can construct the ϕ-cuts from a set of nonuniformly distributed measured data points?

Recently, Rahmat-Samii and Cheung [7] have demonstrated that a two-dimensional nonuniform sampling technique which utilizes irregularly spaced samples (amplitude and phase) can be used to generate the far-field patterns. The mathematical developments of this two-dimensional nonuniform sampling technique have been detailed in [7]. Additionally, a powerful simulation algorithm has then been developed to test the applicability of this sampling technique for a variety of reflector measurement configurations. For example, Figs. 22 and 23 show the simulated nonuniform sample points and the reconstructed far-field patterns in specified ϕ-cuts for a 20 meter offset reflector antenna with a defocused feed operating at L-band [7]. In these figures the solid curves are reconstructed co-polar and cross-polar patterns using the nonuniform sampling technique. It is noted that even though no sample points are captured in these cuts, the reconstructed patterns agree well with the ideal patterns in the angular range where the nonuniform sample points have been generated. Many tolerance studies have also been performed to demonstrate the required measurement accuracies in applying the nonuniform sampling technique [7].

To validate the accuracy of nonuniform sampling technique for antenna pattern construction, several measurements have been performed as reported in [15]. In one of the measurements JPL's 1200-ft far-field range was used, where a 1.47-m circularly polarized Viking reflector antenna (Fig. 24) was measured at X-band (8.415 GHz) using a corrugated horn as the illuminating antenna. The far-field

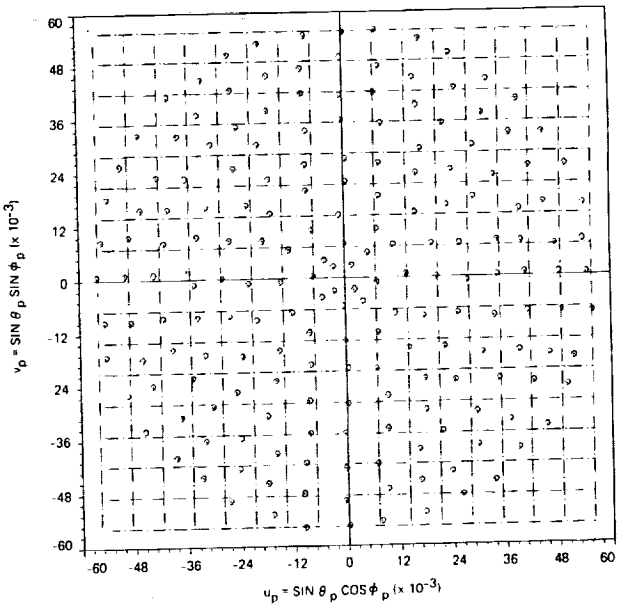

FIG. 22. One hundred ninety two nonuniform sampled point distribution in (u,v) coordinates which covers an angular region of $\theta = \pm 3.2$ degrees.

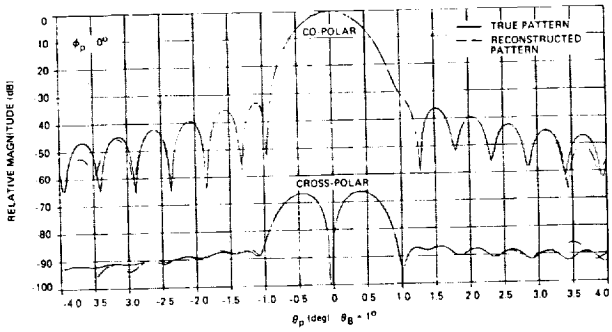

FIG. 23. Far-field patterns reconstructed using nonuniform sampling technique.

amplitude and phase were measured in the directions shown in Fig. 25 which consisted of 585 nonuniformly distributed sampled points in (u,v) coordinates.

The co-polar far-field pattern for $\phi = 90$ degrees is depicted in Fig. 26. The solid curves are the standard azimuth cuts and the dashed curves are the reconstructed patterns using the nonuniform sampling technique. These patterns are constructed by utilizing the window concept as discussed in [7,15]. Note that asymmetric patterns have resulted even though a symmetric reflector was used. this is due to the feed and strut blockage effects. In the angular range of 16.8 degrees where the measured data are available, the comparison between the solid and dashed curves demonstrates close agreement. Note that even though no sampled point has been used at the boresight, the peak of the beam has been reconstructed very well.

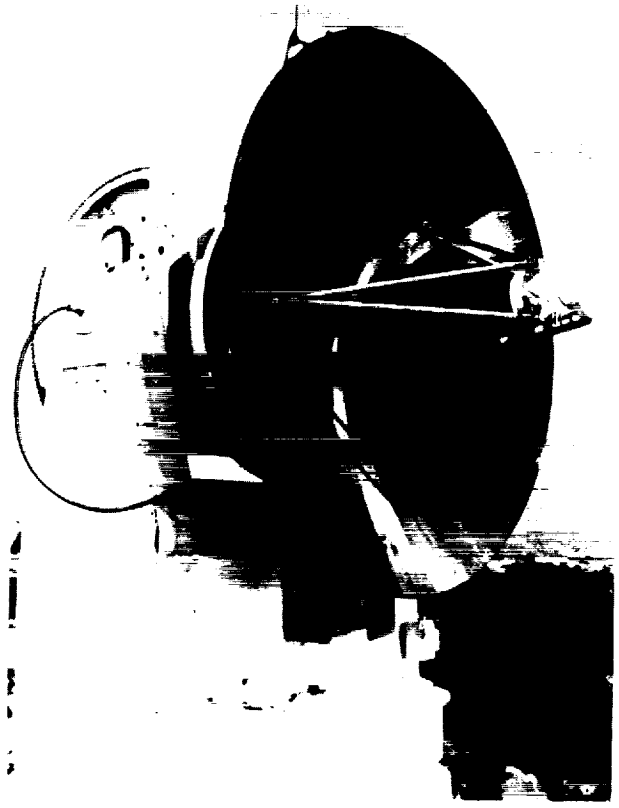

FIG. 24. The 1.47-m circularly polarized Viking reflector antenna operating at X-band (8.415 GHz).

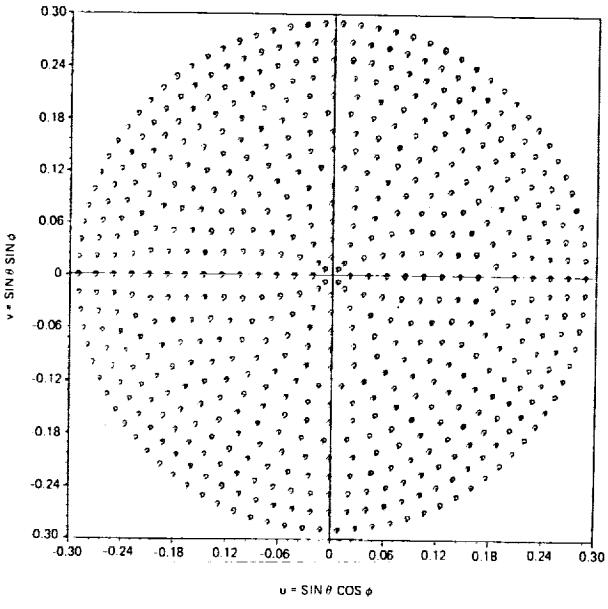

FIG. 25. Five hundred eighty five measured data point distribution in (u,v) coordinates which covers an angular region of $\theta = \pm 16.8$ degrees.

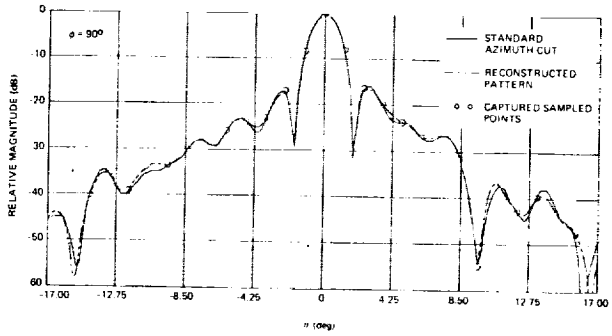

FIG. 26. Reconstructed co-polar far-field patterns of the Viking reflector at X-band using nonuniformly distributed measured data.

6. ANTENNA DISTORTION COMPENSATION

Recent communication system demands require application of very large antennas. Furthermore, it is anticipated that these antennas produce high gain and low sidelobes for future multiple beam satellites. Among different antenna concepts, reflectors still enjoy more acceptance among the designers of large antenna configurations. However, in the space environment the surface of these large reflectors will be distorted resulting in degraded antenna performance [5].

It is very likely that large antennas will suffer from distortions regardless of how rigid the antenna construction is. For this reason, application of an apparatus which would be able to compensate for the distortion will be highly desirable provided that this apparatus can be implemented in a cost effective manner. Fig. 27 shows the mechanism which results in the antenna performance degradation due to reflector surface distortion. The main cause is the introduction of effective aperture phase errors due to the distortion. Fig. 28 summarizes how a corrective apparatus may be used to compensate for the radiated distorted phase front.

Among different possibilities suggested in Fig. 28, recent investigations have revealed the effectiveness of compensating for reflector surface distortions using array feeds [16,17]. This approach is particularly useful in situations for which the reflector distortion is slowly varying, as is typically the case, for example, with large reflectors subject to thermal or gravitational distortions. Additionally, array feeds can be used to improve wide angle radiation characteristics of antennas or to provide low sidelobes.

As presented in [17], a generalized diffraction analysis computer program has been developed which generates complex excitation coefficients for each feed element and then produces the compensated

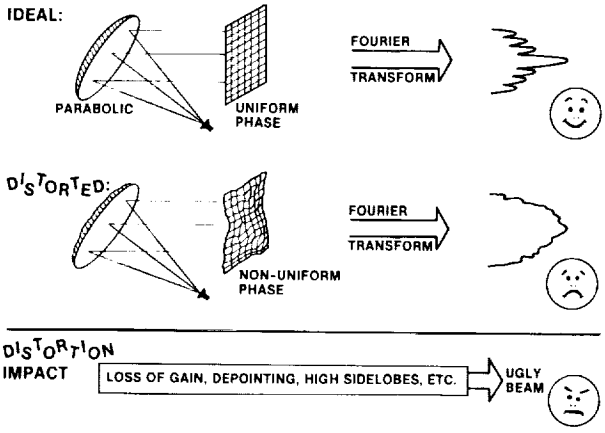

Fig. 27. Schematic presentation of how surface distortions result in degraded antenna performance.

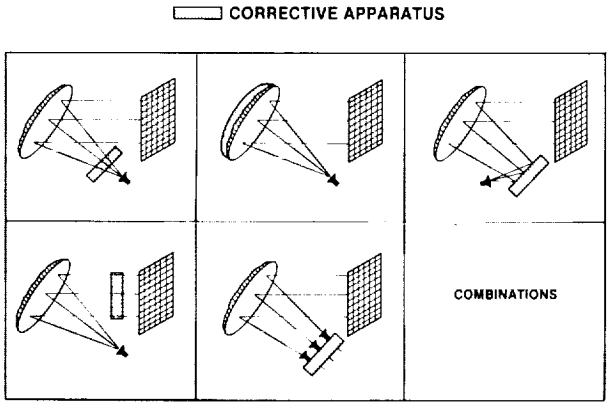

Fig. 28. A conceptual consideration for the utilization of a corrective apparatus.

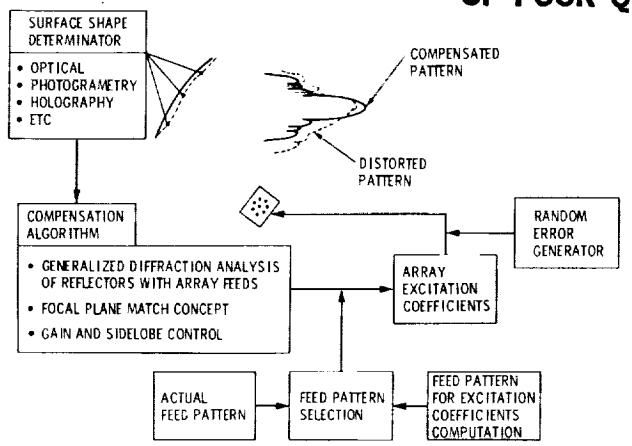

Fig. 29. A generalized block diagram for the incorporation of the array feed compensating algorithm using reflector diffraction analysis.

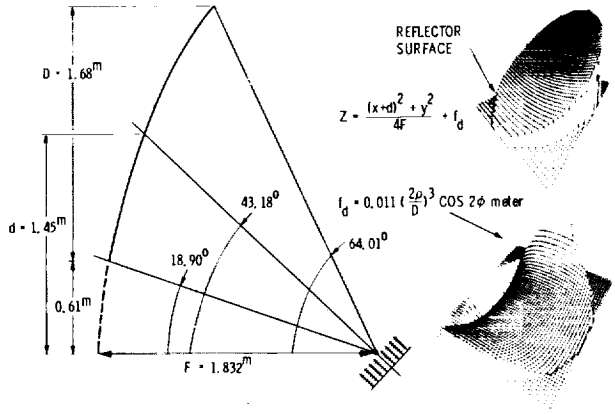

Fig. 30. Reflector surface configuration and its functional representation incorporating slowly varying distortion.

far-field pattern, either for gain or sidelobe control. Fig. 29 depicts the steps necessary to implement this compensating diffraction algorithm.

The concept of conjugate field matching is used to determine the complex excitation coefficients of the array feed. This approach can provide the array excitation coefficients which either maximize the reflector gain in the desired direction or control the sidelobe levels [17]. For the experimental study, it is assumed that the reflector surface is distorted in the fashion shown in Fig. 30, which describes a dominant term in a typical thermal distortion. A pictorial presentation of the reflector surface and its residual deviation from the best fit parabolic surface are shown in Fig. 30. The functional expression in Fig. 30 has been used to fabricate a test reflector in order to demonstrate the utility of the compensation technique via measured data.

A 16-element array feed utilizing cigar elements has been used to perform the experiment (in practice, other array elements such as microstrip elements can be also utilized). Based on this configuration numerical studies were conducted with the results shown in Fig. 31, where significant improvement is achieved using the array feed. Additional numerical studies were performed to identify the accuracies required to position array elements and to set their excitation coefficients; these results were employed in the design of the experiment.

The geometry of the 16-element array feed is shown in Fig. 32. This array consists of 16 cigar elements spaced at 1.06λ (at 8.45 GHz), with an analog phase shifter and variable attenuator behind each element. Since the excitation of each element is set using the corresponding variable attenuator and phase shifter, considerable effort went into proper calibration of this network.

To demonstrate the practical utility of array feeds for the compensation of the

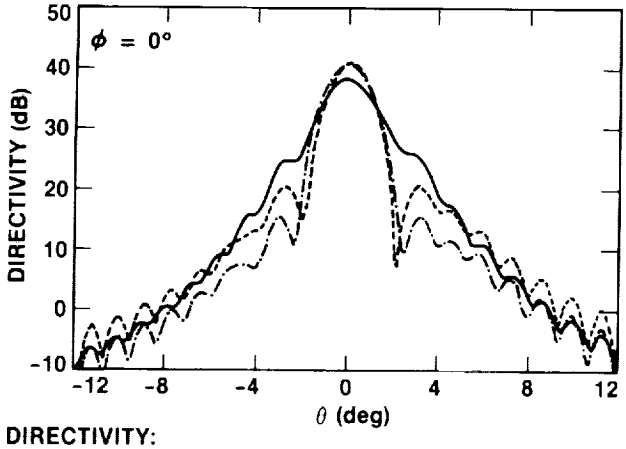

DIRECTIVITY:

——— 38.38 dB (NO COMPENSATION)

----- 40.88 dB (COMPENSATION FOR GAIN)

—·—·— 40.76 dB (COMPENSATION FOR SIDELOBE)

Fig. 31. Compensated and non-compensated far-field patterns generated by diffraction analysis computer program in two different cuts.

ORIGINAL PAGE IS
OF POOR QUALITY

Fig. 32. Sixteen element array feed with attenuator/phase-shifter network (frequency = 8.45 GHz).

slowly varying surface distortions, a reflector with distortion as described previously was used. This reflector was fabricated by the Optical Science Laboratory of the University of Arizona, Tucson, using their Large Optical Generator (LOG) which uses a computer controlled milling machine to accurately contour surfaces. The reflector consists of aluminum honeycomb backing structure surfaced with a machinable foam. After the foam was shaped to the specified profile, a conductive glass fiber material was applied to the surface to make it reflective at microwave frequencies. The steps of this contouring process are shown in Fig. 33.

The photo of this reflector and the 16-element array feed is shown in Fig. 34.

ORIGINAL PAGE
BLACK AND WHITE PHOTOGRAPH

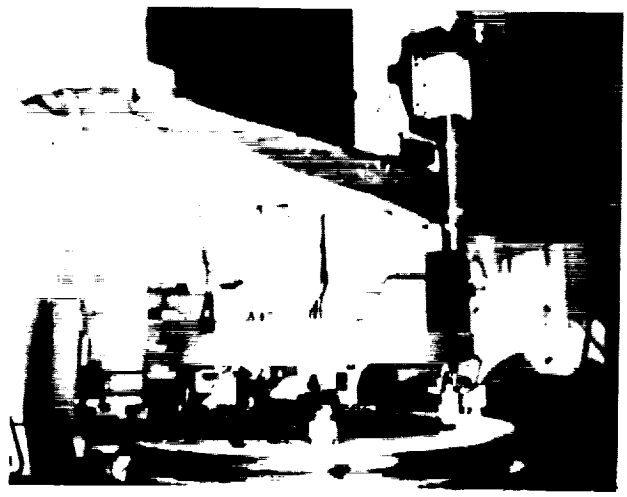

Fig. 33. Surface shaping using the Large Optical Generator (U. of Arizona) to result in a reflector surface as per Fig. 30.

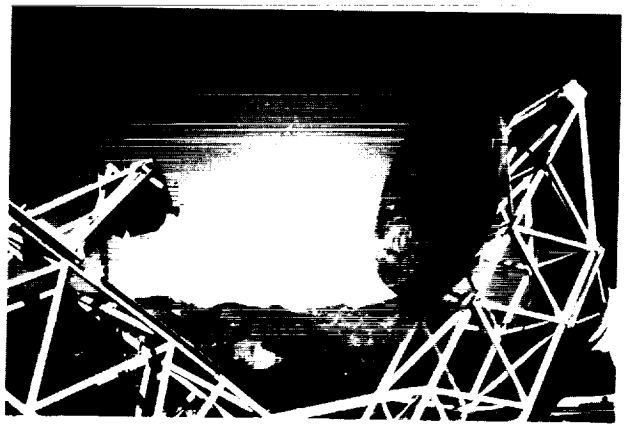

FIG. 34. Distorted reflector and the array feed in the far-field range.

This photo also shows the far-field range where the experiment was performed. The preliminary results of this experiment are presented in Fig. 35 using the steps of the block diagram shown in Fig. 36. Notice that the array feed has improved the reflector performance considerably. The antenna gain has been improved by about 2.5 dB and the antenna patterns have been considerably improved. Additional experiments are being conducted to further improve the sidelobe levels of the compensated patterns.

These results clearly demonstrate the applicability of an adaptive scheme to directly identify the required excitation coefficients of the compensating feed array without actually measuring the reflector surface. This, we believe, is an essential step if such a compensating algorithm is going to be utilized with future large space antennas. It is also anticipated that this compensation technique will be applied to large ground antennas such as Deep Space Network (DSN) antennas.

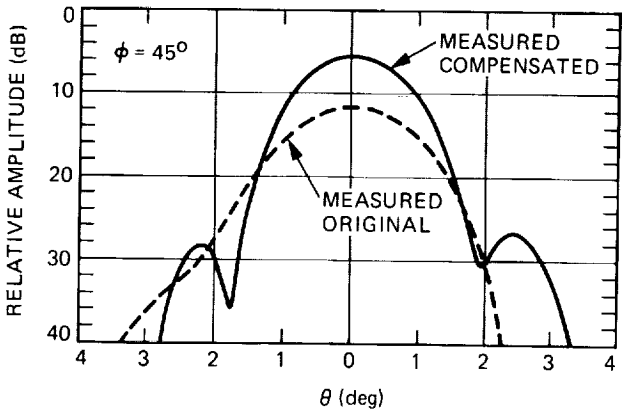

FIG. 35. Comparison between measured patterns for the original and the compensated cases.

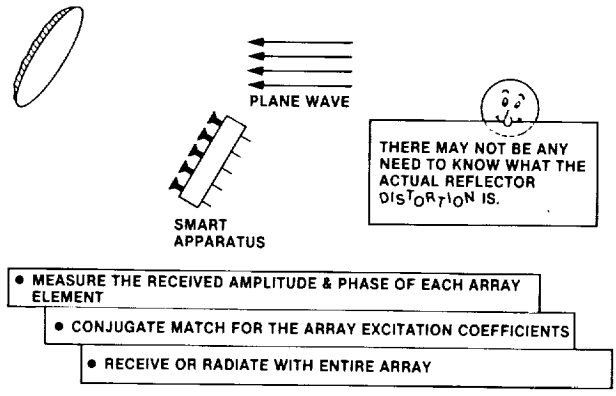

FIG. 36. Steps in implementing an adaptive surface compensation algorithm.

7. ACKNOWLEDGEMENTS

The research described in this paper was carried out at the Jet Propulsion Laboratory, California Institute of Technology, under contract with the National Aeronautics and Space Adminstration. The author would like to thank his colleagues at JPL for their helpful discussions during the preparation of this manuscript.

8. REFERENCES

1. Bennet J. C., "Recent developments in near-field antenna measurements," IEE Fifth International Conference on Antennas and Propagation, ICAP 87, pp. 476-472, York, U.K., April 1987.

2. Johnson R. C., et al, "Compact range techniques and measurements," IEEE Trans. Antennas Propagat., vol. 17, pp. 568-576, Sept. 1969.

3. Rahmat-Samii Y., "Microwave Holographic Metrology for Antenna Diagnosis," IEEE Antenna & Propagat. Newsletter, vol. 29, pp. 5-16, June 1987.

4. Fraser C. F., "Photogrammetric measurement of antenna reflectors," Antenna Measurement Techniques Association Meeting, pp. 374-379, Seattle Washington, Sept. 1987.

5. Rahmat-Samii Y., "Effects of deterministic surface distortions on reflector antenna performance," Annales Des Telecommunications, vol.40, no. 7-8, pp. 350-360, August, 1985.

6. Rahmat-Samii Y., "Vector diffraction analysis of reflector antennas with mesh surfaces," IEEE Trans. Antennas Propagat., vol. 33, pp. 76-90, Jan. 1985.

7. Rahmat-Samii Y. and R. Cheung, "Nonuniform sampling techniques for antenna applications," IEEE Trans. Antennas Propagat., vol. 35, pp. 268-279, 1987.

8. Rahmat-Samii Y. and M. Gatti, "Far-field patterns of spaceborne antennas from plane-polar near-field measurements," IEEE Trans. Antennas Propagat., vol. 33, pp. 638-648, 1985.

9. Baily M. C., et al, "Near-field test results and plans for the 15-meter hoop-column antenna," Antenna Measurement Techniques Association Meeting, pp. 230-234, Seattle Washington, Sept. 1987.

10. Rahmat-Samii Y., "A combined scanning configuration for near-field antenna measurements," NASA Tech Brief, vol. 10, no.5, pp. 44-45, Sept./Oct. 1986.

11. Bolomey J. Ch., et al, "Reduction of near-field techniques duration," Antenna Measurement Techniques Association Meeting, Sept., 1986.

12. Godwin M. P., et al, "Improvement of the Effelsberg 100 meter telescope based on holographic reflector surface measurement," Astron. Astrophys., vol 167, pp. 390-394, 1986.

13. Mayer C. E., et al, "A holographic surface measurement of the Texas 4.9-meter antenna at 86 GHz," IEEE Trans. Instru. Meas., vol. IM-32, pp. 102-109, 1983.

14. Rahmat-Samii Y., "Microwave holography of large reflector antennas -- simulation algorithms," IEEE Trans. Antennas Propagat., vol. AP-33, pp. 1194-1203, 1985 (see minor corrections in vol. AP-34, pp. 853, 1986).

15. Cheung R. and Y. Rahmat-Samii, "Experimental verification of nonuniform sampling technique for antenna far-field construction," Electromagnetics, vol. 6, no. 4, pp.277-300, 1986.

16. Rudge A. W. and D. E. N. Davies, "Electronically controllable primary feed for profile-error compensation of large parabolic reflectors," Proc. IEE, no. 117, pp. 351-358, 1970.

17. Rahmat-Samii Y., "A generalized reflector/array surface compensation algorithm for gain and sidelobe control," 1987 IEEE AP-S Symposium, Blacksburg, VA, June 15-19, 1987.